Journal of Power Sources, 40 (1992) 225–234

Castability of low-antimony/lead battery alloys

Z. W. Chen and J. B. See*
Pasminco Research Centre, Boolaroo, NSW 2284 (Australia)
W. F. Gillian and D. M. Rice
Pasminco Metals, Melbourne, Vic. 3000 (Australia)

Abstract

The castability of three low–antimony (0.8 wt.%, 1.7 wt.% and 2.5 wt.% Sb)–lead battery alloys has been studied using the tree mould approach followed by examination of the cast structure of the grids. For higher antimony contents the castability score was found to be generally higher whilst increasing mould or melt temperatures also increased this score. The combination of grain-refining elements in these alloys was sufficient to refine the grains during casting and the cast structures were basically equiaxed dendritic. The dendritic structure was finer in a downwards direction and towards the end of the branches. This indicates that the running front is likely to be the first to solidify and that flow into the tree mould does not stop due to 'choking'.

Introduction

With the development of low-maintenance and maintenance-free batteries, the use of low-antimony and Pb–Ca–Sn alloys has increased dramatically. The use of these alloys largely reduces or overcomes the problem of electrolyte loss from the batteries associated with high-antimony alloys.

With traditional lead battery alloys manufacturing is relatively easy as these alloys normally contain more than 4% antimony and hence have relatively good castabilities and can be readily age hardened. For low-antimony and Pb–Ca–Sn alloys, problems can occur in handling and the reject rate of grids is increased because of their lowered castabilities and reduced ability to age harden.

Although there have been many studies on low-antimony and Pb–Ca–Sn alloys, there is a lack of detailed information to assist with efficient battery manufacturing. Hence, Pasminco Research Centre is currently conducting a study to generate a complete set of data on the castability and age hardening of low-antimony and Pb–Ca–Sn alloys using experimental conditions simulating those encountered during battery manufacture.

This paper describes part of the results of the study on the castability of low-antimony alloys which are currently widely used in the manufacture of lead/acid batteries.

*Author to whom correspondence should be addressed.

0378-7753/92/$5.00

Experimental procedure

Three low-antimony alloys were used and their composition are listed in Table 1. The values given for each element in the Table are the average of five analyses using a direct-current plasma method except for the values for selenium and sulfur, which are based on two analyses for each alloy by spark spectrometry. Alloy buttons for analysis were taken from the melts and immediately quenched in water during casting. Each alloy was contained in a graphite crucible and melted in an electric furnace. The melt temperature was controlled by an autosetting proportional integral differential microprocessor-based temperature controller.

The castability tree mould approach developed by Mao and Larson [1] was used. This approach closely resembles the practice of gravity casting for battery grids, as it not only considers the fluidity of the melt (the length of the flow before solidification) but it also takes into account the filling capacity of the liquid metal (the ability to fill a mould with complex contours). The mould and the scoring system defined by Mao and Larson are shown in Fig. 1.

The mould temperature was controlled by another autosetting microprocessor-based temperature controller. A K-type thermocouple was used for temperature control

TABLE 1

Compositions for the three low-antimony alloys, wt.%

Alloy	Pb	Sb	As	Cu	Sn	Se	S	Bi
S10	Bal.	2.5	0.24	0.039	0.17	0.012	0.0013	0.008
S20	Bal.	1.7	0.23	0.052	0.18	0.019	0.0016	0.013
S04	Bal.	0.8	0.22	0.049	0.23	0.017	0.0025	0.019

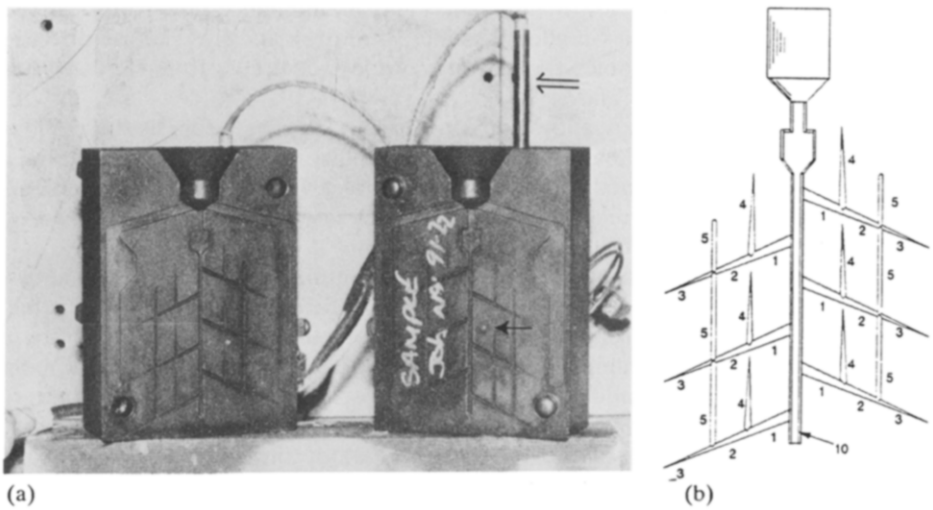

(a) (b)

Fig. 1. (a) Photograph of the castability mould; the arrow with a single tail points to the tip of the thermocouple and the arrows with double tails point to the heating elements. (b) Schematic drawing of the cast cavity and the values assigned to the areas of the mould; a completely-filled mould adds up to 100 points.

with the tip of the thermocouple positioned in the centre of the mould. Two heating elements with a length close to the height of the mould were vertically fixed into both sides of the mould.

After melting the lead alloys and heating the mould to the desired temperature, a specially-made casting cup was immersed in the melt. After the melt temperature returned to the desired temperature, the surface on the melt was skimmed. The casting cup was then quickly taken out and the molten lead alloy poured into the mound. During pouring the tip of the cup was placed as close as possible to the entrance of the casting in the mould. This operation took approximately 3 to 4 s and the pouring procedure was kept consistent.

Casting conditions were varied with three melt pouring temperatures (460, 470 and 480 °C) and three mould temperatures (180, 200 and 220 °C). Three castings were made for each casting condition for each alloy. For grids whose cast structure was later examined, the mould was immediately opened after pouring. The grids were quickly taken from the mould and quenched in ice water.

Cross sections were cut at typical positions for the cast grid samples produced with a pouring temperature of 470 °C and a mould temperature of 200 °C. During cutting, water was run onto the samples and they were then cold mounted using Struers Epofix. After 24 h setting time, the mounted samples were polished using silicon carbide paper down to a fineness of 4000 μm. The samples were then chemically polished (acetic acid plus hydrogen peroxide) and etched (ammonium molybdate and citric acid in water). The microstructure was examined using an optical microscope.

Results and discussion

Castability scores

Table 2 lists the castability scores and 90%-confidence intervals for the three low-antimony alloys. Comparison of the data in Table 2 indicates that increasing antimony content generally increases the castability score. This is better illustrated in Figs. 2 and 3 in which castability has been plotted as a function of antimony content. Figure 2 also shows that increasing melt temperature (left plot through the middle plot to right plot) generally increases the castability score. Figure 3 shows the same effect for increased mould temperature.

The scoring system developed by Mao and Larson (Fig. 1(b)) may have a limitation in that only completely-filled branches score and no score is given to partially-filled branches regardless of whether they are 10%-filled or 90%-filled. For a score of around 30, often 1 or 2 of the 3 point branches can either be completely filled (3 points each) or nearly completely filled (0 point each) for the same casting conditions. Therefore, a confidence (90%) interval of around 3 for a score of 30 can be considered to be very good.

For a higher total score there is more uncertainty about whether a particular branch will be filled or not. Therefore, confidence intervals of 7 to 8 for a castability score of 40 and 13 to 14 for a castability score of 50 can still be considered very reasonable. The majority of the data listed in Table 2 therefore seem reasonable.

The fluidity test has been used in the past to assess the castability of lead alloys. This test measures the length of the molten metal flow in a spiral channel whilst superheat or the difference between the pouring temperature and the liquidus is kept constant.

Heubner and Ueberschaer [2] summarized fluidity data for Pb–Sb alloys as shown in Fig. 4. These data show that, in general, the fluidity decreases with increasing

TABLE 2

Castability score for (a) alloy S10, Sb = 2.5 wt.%, (b) alloy S20, Sb = 1.7 wt.% and (c) alloy S04, Sb = 0.8 wt.%

Mould temperature (°C)	Melt temperature (°C)		
	460	470	480
(a) S10			
180	32.0 ± 2.9	36.7 ± 2.6	36.3 ± 8.5
200	37.0 ± 0.0	41.3 ± 3.9	44.0 ± 6.7
220	49.7 ± 10.2	48.7 ± 4.9	51.0 ± 14.7
(b) S20			
180	32.0 ± 2.9	29.0 ± 2.9	32.3 ± 2.9
200	35.0 ± 2.9	39.3 ± 12.2	38.0 ± 2.9
220	40.7 ± 5.9	40.0 ± 11.8	52.7 ± 4.9
(c) S04			
180	29.0 ± 2.9	32.0 ± 5.8	31.0 ± 5.1
200	29.0 ± 2.9	31.3 ± 5.1	39.0 ± 2.9
220	30.0 ± 2.9	36.0 ± 10.5	42.3 ± 6.8

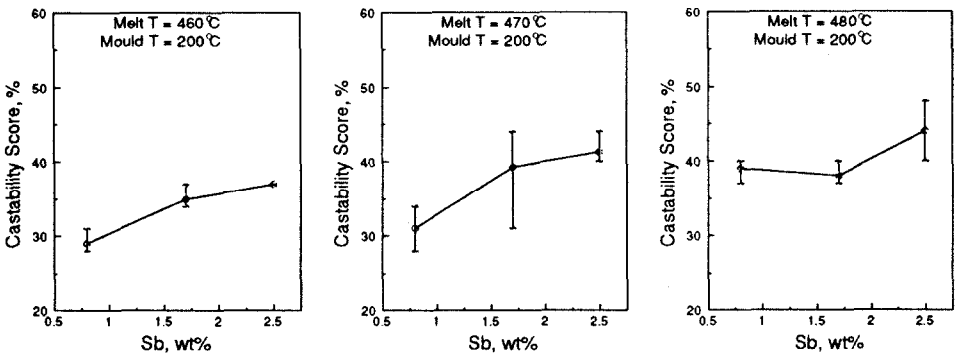

Fig. 2. Castability score as a function of antimony content with constant mould temperature (200 °C) and melt temperatures as indicated.

antimony content for the low-antimony range. There are some differences for data from different workers and this most probably due to the differences in experimental conditions. The decrease in fluidity can probably be explained by the more dendritic structure observed with higher antimony contents. According to Flemings [3], the presence of more dendrites creates more resistance to fluid flow, resulting in lower fluidity.

In a fluidity test, the influence of mould design on the filling capacity of the mould is not considered. The filling capacity may be important for grid casting, especially in thin grid sections in which the surface tension of the running melt during casting may predominate in controlling the flow. In a fluidity test, the cross section of the channel is normally large so that solidification is the major factor stopping the flow of melt.

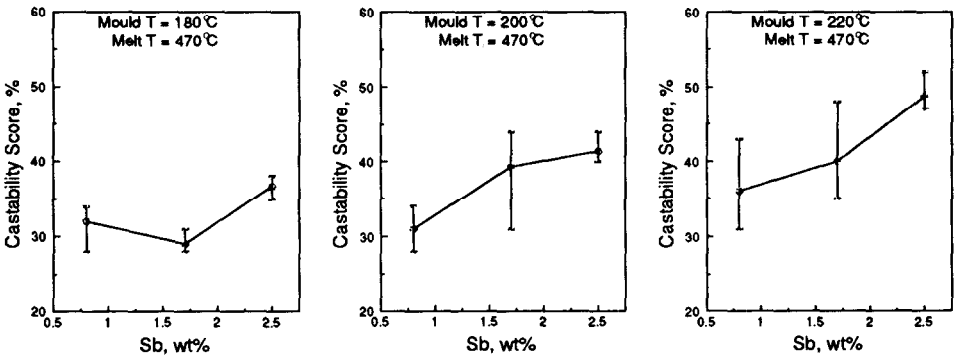

Fig. 3. Castability score as a function of antimony content with constant melt temperature (470 °C) and mould temperatures as indicated.

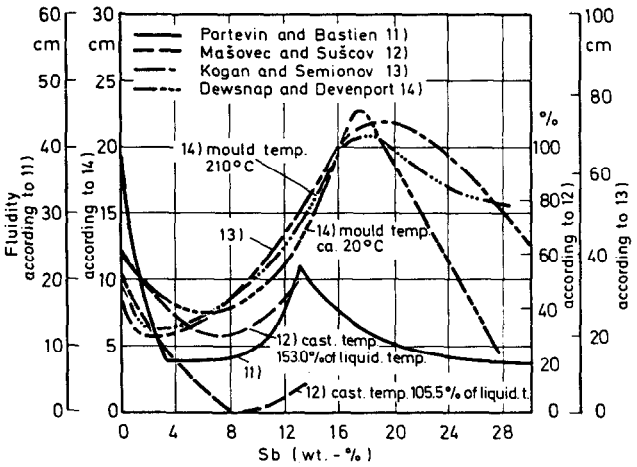

Fig. 4. Fluidity as a function of antimony content in Pb–Sb alloys as summarized by Heubner and Ueberschaer [2]. Reference numbers cited in the graph are the same as in Heubner and Ueberschaer's paper.

Mao *et al.* [4] carried out a test for 4.5 wt.% and 7 wt.% antimony alloys using a castability tree mould to study the influence on castability scores of arsenic additions of less than 1%. They used a melt temperature of 482 °C and a mould temperature of 204 °C, which are very similar to our casting conditions. Their data clearly show that, with or without the arsenic additions, the castability is considerably higher for 7 wt.% Sb–Pb than for 4.5 wt.% Sb–Pb. This contradicts the fluidity data in Fig. 4.

To more easily compare castability-score data to fluidity data, Fig. 5 gives the castability score as a function of antimony content for similar superheats. Figure 5 shows that in general there is still a slight increase with higher antimony contents.

The likely explanation of the castability data, the low-antimony alloy is that a higher antimony content gives a freezing range at lower temperatures. At a given pouring temperature and mould temperature, the time for liquid to completely solidify

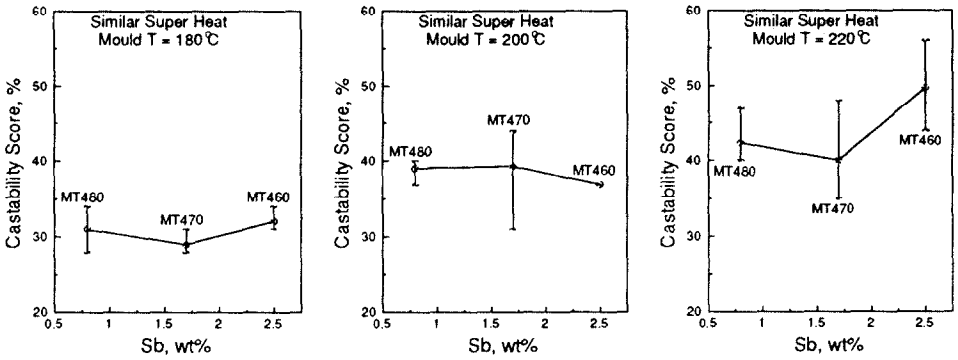

Fig. 5. Castability score as a function of antimony content with similar superheats (~150 °C) and mould temperatures as indicated; (MT470: 470 °C melt temperature, etc.).

is longer for an alloy with the freezing range at lower temperatures. This may compensate for the slightly higher resistance to flow due to more dendritic solidification.

Cast structure

Typical cast structures are presented in Figs. 6–8. It is clear from the micrographs given in the three figures that the structures are almost fully equiaxed dendritic although in places adjacent to the mould wall, and particularly in corners, a slightly more columnar structure is found. The equiaxed dendritic nature of the cast structure indicates that the combinations of grain-refining elements present in the alloys sufficiently refine the grains during casting.

Slightly finer dendritic structures are observed downwards and towards the end of the branches as show by the micrographs of Figs. 6–8. The dendritic sizes (secondary arm spacing) in position C are generally finer than those in position B, whilst the dendrite sizes in position B are finer than those in position A.

Finer dendritic structure or smaller secondary dendritic arm spacing is the direct result of a higher cooling rate or shorter local solidification time [5]. Hence, it is concluded that the running front is subjected to a higher cooling rate during pouring of the melt.

Due to the effect of grain refiners, fine dendritites gradually solidify and are carried along the running front. The flow can therefore be blocked by sufficient solid at the front as occurs in the solidification of grain-refined alloys [5]. Therefore, 'choking', solidification which begins at the casting entrance and is associated with columnar solidification, is not the mechanism that stops flow during casting.

By comparing the structures shown in Figs. 6–8, the cast structure of S10 seems more dendritic in that the dendritite arms are thinner and longer when compared with those of the lower-antimony alloys. Exact explanation of this behaviour is difficult. According to Kurz and Fisher [6], sharper dendritic tips can grow more rapidly because they can reject solute and heat more efficiently. Higher antimony contents would therefore favour the growth of sharper tips or thinner arms as more antimony needs to be rejected during dendritic growth. This probably also explains the thinner arms of the structure in places where heat is readily extracted such as the mould wall and

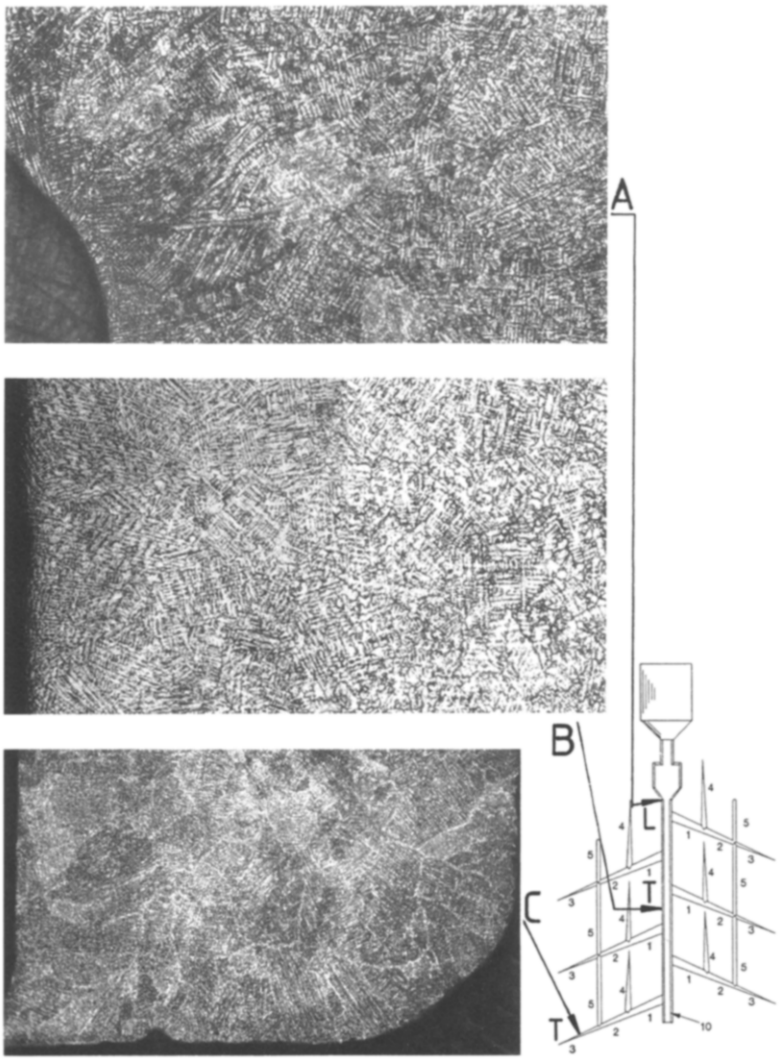

Fig. 6. Microstructure of cast S10 (2.5 wt.% Sb) alloy with pouring temperature 470 °C and mould temperature 200 °C, ×100. L means longitudinal cross and T means transverse cross sections.

the more globular cast structure towards the centre of the cross section, from which heat is more difficult to extract.

The higher the antimony content the lower the temperature at which solidification starts. Therefore, there is a higher loss of grain refiners due to precipitation before the melt solidifies. Hence, it is possible for grain-refining elements to be less effective for an alloy with higher amounts of antimony. This temperature difference of approximately 10 °C is very small and is not likely to have a major effect on the function of the grain refiners and hence on dendritic growth.

However, it should be noted that the effective grain-refining elements, selenium and sulfur, seem to be lower in alloy S10 (Table 1). The copper content is also lower.

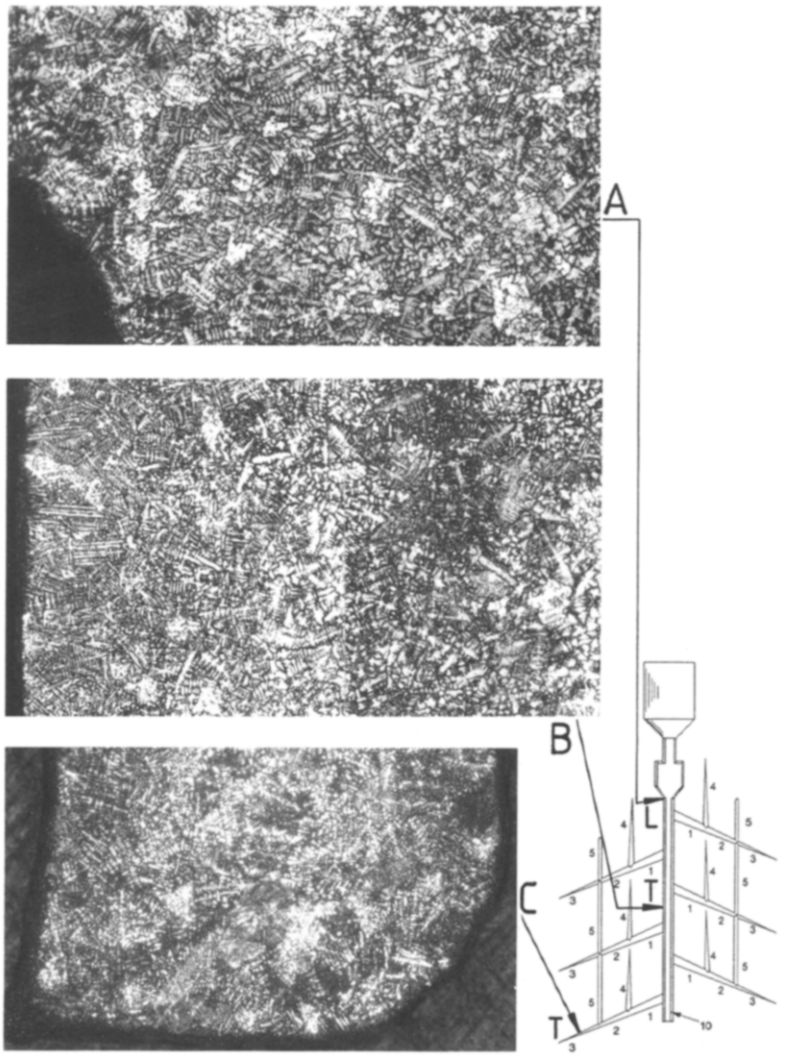

Fig. 7. Microstructure of cast S20 (1.7 wt.% Sb) alloy with pouring temperature 470 °C and mould temperature 200 °C, ×100. L means longitudinal cross and T means transverse cross sections.

This difference in the amount of grain refiners, although it is only slight, hinders the more precise assessment of the effect of antimony content alone. The lower amounts of grain refiners in alloy S10 may have assisted the development of the better defined dendritic structure.

A well-defined dendritic structure has a tendency towards hot tearing if there has been little interdendritic flow during solidification. Although alloy S10 seems to have a better defined dendritic structure, its higher antimony content also means that there is a greater amount of eutectic for interdendritic flow during solidification. Therefore, the tendency for hot-tearing cannot be judged simply by the apparent cast structure obtained for the three alloys.

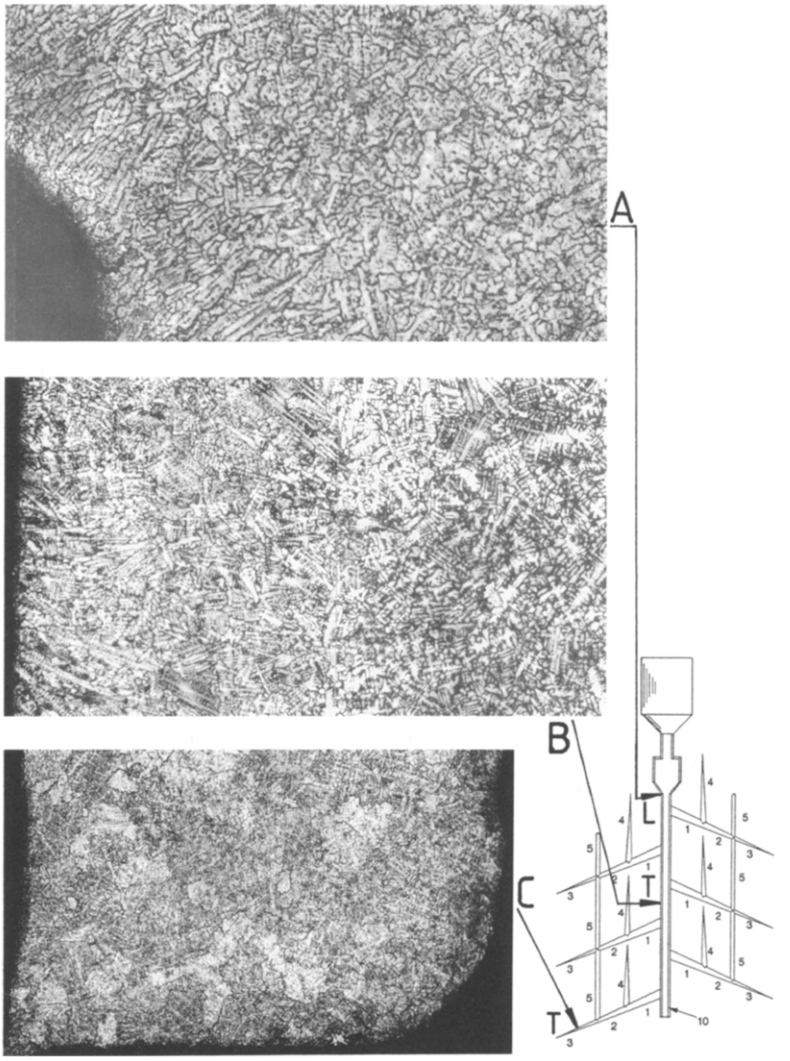

Fig. 8. Microstructure of cast S04 (0.8 wt.% Sb) alloy with pouring temperature 470 °C and mould temperature 200 °C, ×100. L means longitudinal cross and T means transverse cross sections.

Conclusions

1. The castability score determined using the castability tree mould approach generally increases with increasing antimony contents for low-antimony alloys. This does not agree well with data from the fluidity test cited in the literature.

2. Increasing mould or melt temperatures tend to increase the castability score. This applies for all the antimony alloys investigated.

3. The combination of grain-refining elements in the low-antimony alloys sufficiently refines the grains during casting and the cast structures are basically equiaxed dendritic.

4. The dendritic structure is normally finer in a downwards direction and towards the ends of branches. This indicates a higher cooling rate in the running front of liquid before solidification and that the running front is likely to be the first to solidify.

Acknowledgements

The authors would like to thank the senior management of Pasminco Metals and Pasminco Research Centre for permission to publish this paper. Contributions by Mr P. Sargeant to the experimental work are gratefully acknowledged.

References

1 G. W. Mao and J. G. Larson, *Metallurgia,* Dec. (1968) 236–245.
2 U. Heubner and A. Ueberschaer, *Proc. 5th Int. Lead Conf., Nov. 18–22, 1974, Paris,* Bourne Press, England, 1976, pp. 1–8.
3 M. C. Flemings, *Solidification Processing,* McGraw-Hill, New York, 1974, pp. 219–224.
4 G. W. Mao, J. G. Larson and P. Rao, *J. Inst. Met., 97* (1969) 343–350.
5 M. C. Flemings, *Solidification Processing,* McGraw-Hill, New York, 1974, pp. 146–154.
6 W. Kurz and D. J. Fisher, *Fundamentals of Solidification,* 3rd ed., Trans Tech. Publications, Aedermannsdorf, Switzerland, 1989, p. 74.